Draft version March 15, 2013
Preprint typeset using LaTeX style emulateapj v. 5/2/11

arXiv:1303.3350v1 [astro-ph.GA] 14 Mar 2013

VARIATIONS OF MID AND FAR-IR LUMINOSITIES AMONG EARLY-TYPE GALAXIES: RELATION TO STELLAR METALLICITY AND COLD DUST

William G. Mathews[1], Pasquale Temi[2], Fabrizio Brighenti[3,1], Alexandre Amblard[2]

Draft version March 15, 2013

ABSTRACT

The Hubble morphological sequence from early to late galaxies corresponds to an increasing rate of specific star formation. The Hubble sequence also follows a banana-shaped correlation between 24 and 70 micron luminosities, both normalized with the K-band luminosity. We show that this correlation is significantly tightened if galaxies with central AGN emission are removed, but the cosmic scatter of elliptical galaxies in both 24 and 70 micron luminosities remains significant along the correlation. We find that the 24 micron variation among ellipticals correlates with stellar metallicity, reflecting emission from hot dust in winds from asymptotic giant branch stars of varying metallicity. Infrared surface brightness variations in elliptical galaxies indicate that the K - 24 color profile is U-shaped for reasons that are unclear. In some elliptical galaxies cold interstellar dust emitting at 70 and 160 microns may arise from recent gas-rich mergers. However, we argue that most of the large range of 70 micron luminosity in elliptical galaxies is due to dust transported from galactic cores by feedback events in (currently IR-quiet) active galactic nuclei. Cooler dusty gas naturally accumulates in the cores of elliptical galaxies due to dust-cooled local stellar mass loss and may accrete onto the central black hole, releasing energy. AGN-heated gas can transport dust in cores 5-10 kpc out into the hot gas atmospheres where it radiates extended 70 micron emission but is eventually destroyed by sputtering. This, and some modest star formation, defines a cycle of dust creation and destruction. Elliptical galaxies evidently undergo large transient excursions in the banana plot in times comparable to the sputtering time or AGN duty cycle, 10 Myrs. Normally regarded as passive, elliptical galaxies are the most active galaxies in the IR color-color correlation.

1. INTRODUCTION

In a series of recent papers we describe observations and interpretations of far infrared emission from dust in early-type galaxies, emphasizing emission from dust that is in thermal contact with hot gas virialized in galactic or group potential wells (Temi, Brighenti & Mathews 2005; 2007a,b; 2008; 2009a,b = TBM05; TBM07,a,b; TBM08; TBM09a,b). We propose that interstellar dust is ejected and stripped from asymptotic giant branch (AGB) stars as they orbit through the hot interstellar gas ($T \approx 10^6 - 10^7$K). Interstellar dust is heated both by diffuse galactic starlight and by impacts of thermal electrons. The loss of thermal energy by electron-grain impacts can cool gas near black holes in the galactic cores, possibly stimulating energetic feedback events (Mathews & Brighenti 2003). Dust both influences and is influenced by AGN events. In addition, mid infrared circumstellar emission observed in elliptical galaxies is emitted by hotter dust associated with outflows from mass-losing AGB stars.

When mid (24μm) and far (70μm) infrared luminosities from galaxies of all types are compared and normalized by the K-band luminosity, L_{24}/L_K and L_{70}/L_K, galaxies of all Hubble types occupy a remarkably well-defined banana-shaped correlation. Remarkably, the galactic Hubble sequence is ordered along the correlation from early to late morphologies (TBM09b). For spiral and irregular galaxies this color-color correlation results from increasing specific star formation toward later type galaxies. Evidently, dust heated to a range of temperatures by young stars emits mid and far infrared radiation in nearly the same proportion, independently of the specific star formation rate.

By contrast, early-type elliptical galaxies, in which star formation is small or absent, are contiguous with the earliest spiral galaxies in the color-color plot and occupy an extended region of decreasing $\log(L_{70}/L_K)$ with nearly constant $\log(L_{24}/L_K) \approx 30.2$. In general, mid and far infrared emission from dust grains in early-type galaxies does not indicate the star formation rate.

Here we discuss an improved, sharper version of the banana color-color plot for normal galaxies in which galaxies with concentrated mid infrared emission (probably mostly AGNs) are removed. In addition, we propose possible explanations for the cosmic scatter among elliptical galaxies in the infrared color-color plot.

2. THE BANANA PLOT

The top panel of Figure 1, taken from TMB09b, shows the banana-shaped (L_{24}/L_K)-(L_{70}/L_K) plot for nearby galaxies observed in the Spitzer Infrared Nearby Galaxies Survey (SINGS; Kennicutt et al. 2003). In Figure 1, and subsequently, L_{24} and L_{70} are in cgs units and L_K is in solar units. The infrared Spitzer band luminosities at 24 and 70μm are defined by $L_\lambda = \lambda F_\lambda 4\pi D^2$ where D is the distance. The SINGS sample was selected to represent nearby normal galaxies of all morphological types. The

---

[1] University of California Observatories/Lick Observatory, Board of Studies in Astronomy and Astrophysics, University of California, Santa Cruz, CA 95064 (mathews@ucolick.org).

[2] Astrophysics Branch, NASA/Ames Research Center, MS 245-6, Moffett Field, CA 94035 (pasquale.temi@nasa.gov).

[3] Dipartimento di Fisica e Astronomia, Università di Bologna, via Ranzani 1, Bologna 40127, Italy (fabrizio.brighenti@unibo.it).

banana-shaped plot in the top panel of Figure 1 provides an infrared main sequence for the Hubble classification. Colors in Figure 1 (top) designate five morphological types using the de Vaucouleurs T parameter from HyperLeda (Paturel et al. 2003). The morphological type varies rather smoothly along the banana from early types at the lower left to the latest galaxies at the upper right: E → Sa,Sab → Sb,Scd → Irr. Proceeding upward in Figure 1, the luminosity ratio $L_{24}/L_K \propto (L_{70}/L_K)^{1.2}$ is a surrogate for an increasing specific star formation rate (SFR) from early to late types (Calzetti et al. 2007). S0 galaxies have SFRs that vary from essentially zero, similar to red and dead E galaxies, to rates typical of irregular galaxies having the highest specific SFRs (TBM09a), i.e. S0s can be found all along the banana.

The galaxy sample discussed by TBM09b, selected from the Spitzer archive, is rich in early type galaxies, complementing the emphasis on later types in the SINGS data. The central panel of Figure 1, which combines these two data sets, shows that the lower region of the banana occupied by E and E-S0 galaxies is quite extensive and possible reasons for this extension are discussed below.

Recently we discovered that many of the outlying galaxies in the TBM09b sample displaced above the banana (indicated with green squares in Figure 1) exhibit strongly concentrated 24μm emission. This concentration is apparent from the visibility of Airy rings in 24μm images, including additional angular artifacts characteristic of MIPS diffraction at this wavelength (see also Calzetti et al. 2010). While it is possible that 24μm diffraction in some galaxies may be due to centrally concentrated starbursts, most of the galaxies with Airy rings have been previously identified as having additional independent evidence of AGN activity. Moreover, in the central panel of Figure 1 it is seen that galaxies having Airy rings (green squares) lie above the banana correlation *almost everywhere along the banana.* If concentrated starbursts are responsible for Airy rings, the star formation trajectory in Figure 1 of dust heated in unresolved starbursts would need to be *steeper* than the locus of star formation along the upper banana, $\delta\log(L_{24}/L_K)/\delta\log(L_{70}/L_K) \approx 1.2$, which seems unlikely. For these reasons, we argue that harder AGN radiation, not concentrated starbursts, is the most likely explanation for the 24μm Airy rings. All early-type galaxies with Airy diffraction probably have low-level active nuclei (Tang et al. 2009)

The top row of three panels in Figure 2 illustrates 24μm images of two galaxies with visible Airy rings, NGC 1386 and NGC 0315, and one, NGC 4472, which has no detectable Airy diffraction. Galaxies in Figure 1 with significant visible Airy rings are listed in Table 1. Centrally normalized surface brightness profiles are shown in the lower panel of Figure 2 together with the Spitzer point response function at 24μm, which decreases to half its central value at about 3.4 arcseconds. When (AGN) galaxies with strong 24μm Airy rings are removed, as in the bottom panel of Figure 1, the infrared color-color banana plot becomes much tighter.

2.1. *Bottom of the Banana*

Figure 3 shows an expanded view of galaxies that occupy the bottom, rather flat part of the banana, most or all of which are E or E-S0 galaxies ($T < -2.7$). Galaxies with strong **central** point source emission at 24μm have been removed. Of particular interest is the large extent of the region occupied by early type galaxies, having an intrinsic scatter that exceeds the errors of observation (e.g. as shown in the vertical error bars in Fig. 4). If these elliptical galaxies are dominated by old stellar populations, one might imagine that they would occupy a much smaller region in the banana plot. We now discuss in turn the physical origin of the vertical (L_{24}/L_K) and horizontal (L_{70}/L_K) scatter of early-type galaxies in Figure 3. The outlying galaxy with the lowest L_{24}/L_K in Figures 1 and 3 is NGC 4406.

3. INTRINSIC SCATTER OF L_{24}/L_K FOR E GALAXIES: STELLAR METALLICITY

Low mass, oxygen-rich asymptotic giant branch (AGB) stars are thought to dominate the optical luminosity and dust production in elliptical galaxies (e.g. Habing 1996; Athey et al. 2002). Consequently, it is natural to expect that AGB stars having higher metallicity also have more hot circumstellar dust and more emission at 24μm, possibly accounting for the vertical scatter in Figure 3. To test this idea, we use the sample of elliptical galaxies with metallicities $[Z/H]$ determined by Trager et al. (2000a, b), most of which have been observed at 24μm and which are identified with red circles in Figure 3. Relevant properties of Trager's sample are listed in Table 2.

Figure 4 shows that L_{24}/L_K does indeed correlate with stellar metallicity $[Z/H] = \log[(Z/H)_{galaxy}/(Z/H)_\odot]$ is normalized to the solar abundance:

$$\log(L_{24}/L_K) = 29.99 \pm 0.31 + (0.52 \pm 0.16)[Z/H] \quad (1)$$

$$\log(L_{24}/L_K) = 30.12 \pm 0.42 + (0.76 \pm 0.21)[Z/H] \quad (2)$$

Values of $[Z/H]$ in equations (1) and (2) refer respectively to apertures of size $R_e/8$ and $R_e/2$ where R_e is the effective radius in the B-band (Trager et al. 2000b). The correlations in Figure 4 indicate that broadband observations at rest-frame 24μm could be used to determine the stellar metallicity of distant, old-population early-type galaxies at higher redshift, provided there are no strong AGN contributions. The correlation between stellar age and metallicity among elliptical galaxies discussed by Terlevich & Forbes (2002), is not apparent in the galaxies plotted in Figure 4.

3.1. *Metallicity Gradients and 24μm Surface Brightness*

Proceeding further with this idea, can the (negative) stellar metallicity gradients in elliptical galaxies be measured from radial variations in the $K - 24\mu$m color? An initial response to this question appears in Temi, Brighenti, Mathews (2008 = TBM08), and we follow the same data reduction procedure here. In TBM08 we discussed the mean $\langle K-24\rangle$ color profile averaged over a sample of only 19 galaxies, 10 of which are in common with the Trager et al. (2000b) sample. In that paper we found that $\langle K-24\rangle(R)$ decreased linearly with $[Z/H]$ to about $R \approx 1.2R_e(K)$, then flattened, and at $R \gtrsim 1.8R_e(K)$ began to rise again. $R_e(K)$ is the K-band half-light radius. Now with the complete Trager sample, about twice as large, we find a similar mean $\langle K-24\rangle$

differential surface brightness profile shown in the upper panel of Figure 5.

The flattening of $\langle K-24\rangle$ at $0.8 \lesssim R/R_e(K) \lesssim 1.6$ and subsequent rise at larger $R/R_e(K)$ in Figure 5 does not indicate that these elliptical galaxies have bright halos of 24μm emission. Figure 1 of TBM08 shows that the surface brightness profiles of typical elliptical galaxies at all Spitzer infrared wavelengths (including 24μm) deviate rather little from the de Vaucouleurs profiles in optical light. But systematic radial color variations do exist and $\langle K-24\rangle$ is the most unusual. In the lower panel of Figure 5 we convert $\langle K-24\rangle$ into $[Z/H]$ using the linear relation shown in Figure 4 with $[Z/H]$ evaluated in the $R_e/2$ aperture. We assume that the linear behavior in equation 2 can be extrapolated to larger $[Z/H]$. Values of $[Z/H]$ at $R_e/2$ are preferred to match the global luminosities L_{24} and L_K in Figure 4 and because $R > R_e(K)$ for all Z/H values in Figure 5. When $[Z/H]$ values observed at $R_e/2$ are used, the U-shape of the radial variation in the lower panel of Figure 5 is largely unchanged but it is normalized to somewhat larger values of $[Z/H]$.

Optical observations of $[Z/H]$ profiles using the Lick indices at comparable $R/R_e(K)$ invariably indicate monotonically decreasing stellar metallicity with galactic radius and this trend might also be expected in the hot dust emission. But how can the flattening and possible rise in the $[Z/H]$ profile in Figure 5 be explained? If the outer regions of elliptical galaxies are formed by the accretion and disruption of smaller galaxies, then we would expect lower metallicity at large $R/R_e(K)$ typical of smaller galaxies, apparently opposite to the trend in Figure 5. Excess $\langle K-24\rangle$ at large $R/R_e(K)$ could in principle be due to dust acquired by accretion in distant regions of the galactic atmosphere where the gas density (and possibly temperature) is much lower, increasing the grain sputtering time, preserving a higher dust density. However, in normal elliptical galaxies emission at 24μm is dominated by hot dust in circumstellar regions around mass-losing AGB stars, not by emission from much colder interstellar dust grains. (see for example our computed models in Fig. 8).

Does dust in low metallicity AGB winds have higher 24μm luminosities? Computed evolutionary tracks of AGB stars exhibit increasing effective temperature with decreasing abundance (Cristallo et al. 2009). If 24μm-emitting grains are heated by thermal impacts, this increase in effective temperature may be sufficient to account for the enhanced circumstellar 24μm emission at large $R/R_e(K)$ seen in Figure 5. Another possible explanation is that the outflow velocity in AGB stars is reduced (or rendered intermittent) by lowered radiation pressure acting on fewer or smaller grains in low-metallicity AGB stars, increasing the gas density in the AGB outflow, possibly allowing a smaller mass fraction of dust grains to emit disproportionally more in the mid-infrared. If low metallicity is the source of the apparent $[Z/H]$ upturn in Figure 5, it must occur at metallicities lower than those plotted in Figure 4 where no low-$[Z/H]$ upturn is visible.

In any case, the decreasing $\langle K-24\rangle$ at small radii, $R/R_e(K) \lesssim 0.8$, in the upper panel of Figure 5 is consistent with the expected decrease in stellar abundance observed optically in this region. The stellar metallicity gradient in Figure 5 at $R/R_e(K) \lesssim 0.8$, $\Delta[Z/H]/\Delta\log R \approx -0.23$, is in good agreement with previously observed metallicity gradients in elliptical galaxies (Carollo et al. 1993; Davies et al. 1993; Kobayashi & Arimoto 1999; Mehlert et al. 2003; Kobayashi 2004; Koleva et al. 2011).

4. INTRINSIC SCATTER OF L_{70}/L_K: COLD INTERSTELLAR DUST

In the upper part of the banana, where $\log L_{70}/L_K \gtrsim 31.1$ in Figure 1, 24 and 70 micron emission from normal galaxies are dominated by star formation. For $\log L_{70}/L_K \lesssim 31.1$, the 70 micron emission from early-type, mostly E galaxies is a measure of the varying amounts of cold dust in the hot interstellar gas (TBM07a,b).

To discuss horizontal variations and excursions in L_{70}/L_K along the bottom of the banana, we return to the complete galaxy sample shown in the lower panel of Figure 1 and consider only elliptical galaxies. Figure 6 shows the huge range in far infrared luminosity L_{70} for elliptical galaxies ($T < -3.5$) having similar L_K. Galaxies with the largest L_{70} have either undergone dust-rich mergers (such as NGC 5018) or are central galaxies in groups, although some galaxies with the lowest L_{70}, such as NGC 1399, are also group-centered. L_{70} luminosities of NGC 1399 and 4472, both near the Spitzer detection limit, are in excellent agreement with our steady state model for the minimum far infrared emission from interstellar dust ejected from AGB stars into the hot ISM of normal elliptical galaxies as described by TBM07a,b. In this steady state calculation, which we now briefly review, stellar dust is created locally at the same rate that it is consumed by sputtering.

Approximate stellar ages and main sequence turnoff rates in elliptical galaxies can be obtained from Balmer line absorption in optical spectra and photometry. From this follows (1) the mean current stellar mass loss rate from old stellar populations, $dM_*/dt \approx 1.5(M_*/10^{12}M_\odot)$ $M_\odot$ yr^{-1}, and (2) the associated interstellar dust production rate by AGB stars, assuming a metallicity-dependent (dust mass)/(gas mass) ratio normalized to ~ 0.01 at solar abundance. Warm, dusty gas is deposited into the hot ($T \sim 10^6 - 10^7$K) interstellar gas along the ram-pressure stripped wakes of orbiting AGB stars and is subsequently maintained at $T \sim 10^4$K by UV from post-AGB stars. The stripped warm gas must thermally merge into the hot interstellar gas ($T \sim 10^6 - 10^7$ K) in less than about $10^{5.5}$ yrs, otherwise optical Hα emission line luminosities would exceed typical observations (Mathews 1990; Mathews & Brighenti 2003).

Consequently, after $\sim 10^{5.5}$ yrs dust grains can be expected to come into direct thermal contact with the hot gas and begin to be eroded (sputtered) by collisions with H$^+$ and He^{++} ions. A typical grain sputtering lifetime is $\sim 10^7$ yrs at galactic radius $r \sim 5-10$ kpc. Interstellar dust grains are heated in comparable amounts by absorption of local starlight and by inelastic collisions with thermal electrons in the hot gas. Each colliding electron deposits $\sim (3/2)kT$ into the grain.

We assume that dust ejected from AGB stars, has a typical initial grain size distribution $N_0(r,a) \propto a^{-3.5}$ normalized to the local stellar metallicity at galactic radius r. In a steady state, when grain heating-cooling and formation-destruction balance at every galactic radius r, we can determine the temperature $T(r, a)$ of (amorphous silicate) grains of radius a. Integrating over the grain size distribution (altered by sputtering) and the projected surface of the galaxy, we can calculate (TBM07a,b) the total specific luminosity or flux λF_λ in any field of view aperture. By this means the infrared SED can be estimated for any elliptical galaxy based on its luminosity, distance and the temperature and density profiles of hot interstellar gas observed in the X-ray.

We find that the far infrared luminosity observed in certain galaxies – such as NGC 1399 and NGC 4472 – are very close to our steady state predictions (TBM07a). These galaxies are also near the lower limit of elliptical galaxies that can be detected with Spitzer MIPS at 70μm. For these galaxies, the local hot interstellar gas is assumed to consume dust by sputtering at the same rate that it is produced in local AGB outflows. This model can reproduce 70μm and 160μm luminosities for ellipticals with rather low L_{70}, but truly interstellar dust is too cold to emit observable 24μm emission. Evidently, L_{24} is produced exclusively by much hotter dust in AGB outflows, heated only by the nearby parent AGB stars, and this emission is not considered in our dust evolution model.

If interstellar L_{70} emission from all elliptical galaxies agreed with our steady state predictions, they would occupy a disconnected island near $\log L_{70}/L_K \sim 29.0 \pm 0.5$. And observed AGB-heated dust would still dominate 24μm emission from ellipticals with some scatter for variable metallicity, $\log L_{24}/L_K \sim 30.10 \pm 0.15$. Our steady state model predicts that the banana plot would appear only as this island for ellipticals and a separate powerlaw sequence of star-forming galaxies of later types.

However, and to our initial surprise, many optically normal E galaxies – e.g. NGC 4636 and 5044 – have L_{70} that are 10-30 times brighter than our steady state prediction. This infrared excess indicates the presence of excess cold interstellar dust (of mass $\sim 10^5$ $M_\odot$) that cannot have come from local mass-losing stars. In addition, elliptical galaxies with excess L_{70} often have spatially extended far infrared emission, extending beyond the Spitzer 70μm point response function (TBM07a). Galaxies with observationally confirmed extended dust are indicated in Figure 6 with large red circles. The far infrared color L_{160}/L_{70} of observed excess dust emission confirms that this excess dust is located further out in the E galaxy interstellar atmosphere, at $r \sim 5 - 10$ kpc, where grain heating by starlight and electron-grain collisions are diminished (TBM07b). Because of the short dust sputtering lifetime, $\sim 10^7$ yrs, the excess dust emission at these large radii must be transient.

Transient, spatially extended dust can arise (1) from recent mergers or (2) by internally produced dust that is hydrodynamically transported outward from galactic cores with AGN-heated gas. Some elliptical galaxies with the highest L_{70} have acquired dust by a recent merger and sometimes a post-merger dust distribution is clearly visible. In other cases it is difficult to determine if dust is supplied externally for example by minor mergers since these may be difficult to detect without a detailed analysis, as argued by Crockett et al. (2011). Nevertheless, our impression from images of many elliptical galaxies with high L_{70} is that they are not surrounded by small, gas-rich galaxies that are about to merge. If the dust sputtering lifetime $\sim 10^7$ yrs is relevant, such mergers would have to be quite frequent, requiring multiple simultaneous ongoing small mergers to explain for example the extended 70μm image of NGC 5044 (TMB07b). At a few kpc radius, the orbital time of merging galaxies is likely to be longer than the sputtering time of dust stripped from them. In addition, gas-rich merging galaxies must release widespread dust into the hot gas atmosphere that emits 70μm, but star-forming regions in gas-rich merging galaxies must not emit detectable 24μm emission since emission at this wavelength correlates with the stellar metallicity of the host galaxy (Fig. 4). Moreover, dwarf galaxies observed near central galaxies in groups/clusters tend to be free of interstellar gas, due in part to ram stripping in the distant past. For these reasons we consider here the hypothesis that internally produced interstellar dust can explain many elliptical galaxies with excess dust often extending far beyond the effective radius of the central galaxy. In TBM07b we described how dusty, hot interstellar gas can be buoyantly or hydrodynamically transported outward as a result of AGN heating events (feedback) in galaxy cores.

For internally produced dust to explain the extended excess infrared emission in elliptical galaxies, it is essential to have a reservoir of dust near central black holes. This source of dust is conveniently provided by optically thick clouds or disks of dense dusty gas observed in projection against starlight in galactic cores (e.g. van Dokkum & Franx 1995; Lauer et al. 2005). The common incidence of dusty disks or chaotically distributed dusty clouds within the central kpc of many ellipticals indicates that the steady state dust creation-destruction assumption we use to compute extended far-IR dust emission breaks down in dense elliptical cores. Apparently more dust is created in elliptical cores than can be destroyed by local sputtering. Dust in stellar ejecta can radiatively cool ambient hot gas faster than the sputtering or freefall time, as discussed by Mathews & Brighenti (2003). When the central black hole accretes some nearby dust-cooled gas and releases feedback energy, we propose that some of the central dusty gas is heated and flows buoyantly out to 5-10 kpc from the center where it thermally merges with the hot interstellar gas before the dust is sputtered away. We identify these AGN-driven outflows as the source of excess extended far infrared emission observed in many elliptical galaxies shown with red circles in Figure 6.

Figure 7 shows elliptical galaxies ($T < -3.5$) in the bottom of the banana plot in a region similar to Figure 3. Galaxies with red dots in Figure 7 are chosen because of their large L_{70}/L_K for given L_{24}/L_K, lying along the rightmost boundary of the lower banana. These same galaxies are also plotted with red dots in Figure 6 where it is seen that they all have significant excess 70μm emission. Galaxies with red circles in both Figure 6 and 7 are those in which the excess far-IR emission is known to be spatially extended in 70μm Spitzer images (TBM07a,b).

Small open green circles in Figures 6 and 7 show the approximate computed locations of two galaxies – NGC 5044 and NGC 4636 – using our steady-state dust evolution model in which dust ejected from galactic stars is destroyed locally by sputtering. The green arrows illustrate the large additional (excess) contribution to L_{70}

which we interpret as dust in gas heated by AGN feedback events and then transported outward from galactic cores. Without this extended excess dust these two galaxies may not have been detected with Spitzer. Similar displacements probably occurred recently in the other red elliptical galaxies in the banana boundary region of Figure 7.

If our interpretation is correct, group-centered galaxies, like NGC 5044 and NGC 4636, move back and forth along the bottom of the banana in Figure 1 on timescales determined by the grain sputtering lifetime and the interval between AGN outbursts, which may be roughly comparable, $\sim 10^7$ yrs. Elliptical galaxies that are not known to be group-centered can also participate in similar large, transient horizontal excursions in the banana plot, provided their virialized hot gas atmospheres are hot enough ($T \gtrsim 4\times10^6$ K) to sputter and are sufficiently extended. However, there appears to be no correlation between excess 70μm emission and X-ray luminosity (TBM07a).

One potential difficulty with our hypothesis is that no galaxy is observed to lie appreciably further to the right than the group of red dot galaxies in Figure 7. Comparing Figure 7 and the bottom panel of Figure 1, it is seen that the slope of the rightmost envelope of red galaxies in Figure 7 lies just along the star-formation track defined by galaxies of later type ($(L_{24}/L_K) \propto (L_{70}/L_K)^{1.2}$). Somehow, the rightward excursions caused by the outward movement of excess cold dust due to feedback events must be limited so as not to exceed the star-formation locus.

To understand this, we conclude that central star formation must eventually occur when the mass of dusty gas accumulates beyond a certain point in the cores of elliptical galaxies. Star formation causes both L_{70} and L_{24} to increase as elliptical galaxies rise along the SINGS star-forming locus. Star formation and AGN-driven dust transport into the hot gas atmospheres are not mutually exclusive. If central star formation commences, the horizontal green arrows in Figure 7 should bend at the right to move up along the star-formation trajectory with increasing L_{24}/L_K. It is likely that low-level star formation occurs in all elliptical galaxy cores (Ford & Bregman 2012) in dense dusty clouds formed by dust-assisted cooling of gas ejected from AGB stars (Mathews & Brighenti 2003).

A quasi-steady-state cyclic dust evolution that involves reservoirs of increasing dust mass in galaxy cores may explain the large variation in L_{70}/L_K shown in Figures 6 and 7. Cold gas clouds containing optically visible dust slowly accumulate in galaxy cores as gas from stellar mass loss is cooled by dust. Occasionally these dusty clouds may be heated by AGN events to $\sim 10^7$ K and flow out into the surrounding hot atmosphere emitting $70mu$m radiation. Ultimately this extended dust is likely to be sputtered into the gas phase. Such a hypothetical dust evolution could create and destroy dust at approximately balancing rates. Star formation may or may not occur during each feedback episode, and it would also serve to consume some of the accumulated cold gas and dust.

The evolution of optically thick dust clouds in the cores of elliptical galaxies must also participate in the quasi-cyclic production of extended cold dust. If cold dusty gas within the central ∼kpc forms by cooled stellar ejecta as we propose, the default endstate is most likely a small rotating dusty disk. The spin axis of the disk will be aligned with the kinematical minor axis of nearby stars. While such central disks are often observed (e.g. van Dokkum & Franx 1995; Lauer et al. 2005), it is more common to find a multitude of patchy, chaotically distributed dust clouds or no dust absorption at all. Because of the small solid angle presented to the central black hole, thin, cold dusty disks may be difficult to disrupt if AGN energy is released only at the black hole. However, disks may be more easily disrupted by symmetric depositions of AGN energy in bipolar regions somewhat removed from the black hole and misaligned from the disk axis. In this case shock energy reaches opposite sides of the disk at different times, causing mechanical disk disruption. Even if strong shock waves arrive simultaneously on both sides, if the shocks are strong enough, much or all of the disk could be sufficiently heated to merge with the hot gas. While these important details remain unexplored, in at least one case we observe both a relaxed dusty disk with nearby dense clouds presumably from a disrupted previous disk generation. In NGC 5044, where extended dust is resolved at 70μm (TMB07b), the central kpc contains many chaotically distributed optically thick clouds with orbital lifetimes $\sim 10^7$ yrs compatible to the hydrodynamic and sputtering lifetimes of the extended dust (TBM07b). In many cases remnants of disrupted central dusty gas may be too small or too widely dispersed by AGN outbursts to be visible as optically thick clouds.

5. UN-NORMALIZED BANANA PLOT

Figure 8 shows a less compact version of the banana plot in which L_{24} and L_{70} are plotted without normalization with L_K. SINGS galaxies (crosses in Fig. 8) define a star-forming sequence $L_{24} \propto {L_{70}}^{1.08}$ in which L_{24}/L_{70} is approximately constant as L_{24} varies by five orders of magnitude. Many of the Spitzer-archived elliptical galaxies in Figure 8 that occupy the SINGS star-forming region above $\log L_{24} \approx 41.8$ are peculiar.[2] SINGS galaxies in Figure 8 having low star formation rates lie considerably below L_{24} of normal giant elliptical galaxies. The black filled squares in Figure 8 illustrate the very small diffuse interstellar L_{24} emission for five representative ellipticals computed with our steady-state dust evolution.

6. CONCLUSIONS

The banana-shaped infrared color-color correlation for normal galaxies – a plot of $\log(L_{70}/L_K)$ vs. $\log(L_{24}/L_K)$

---

[2] The two elliptical (red) galaxies with $\log L_{24} \sim 42.6$ (NGC 807 and UGC 01503) in Figure 8 have massive ($\sim 10^9\ M_\odot$) multi-kpc rotating dusty HI disks (Goudfrooij et al. 1994; Young et al. 2009; Young 2002), likely to be old mergers. NGC 3125 (at $\log L_{24} \approx 42.26$) is a compact dwarf galaxy ($\sigma = 48$ km s^{-1}) with strong emission lines (Koprolin and Zeilinger 2000). Very little is known about NGC 4786 ($\log L_{24} \approx 42.26$). The group of five E galaxies at $\log L_{24} \approx 41.92$ includes NGC 5018 [with a large $\sim 10^8\ M_\odot$ filament of dusty HI gas], NGC 3557 [an FRI radio source (Birkinshaw & Davies 1985) with extended Hα emission (Goudfrooij et al. 1994)], NGC 4125 [with a central X-ray source (Flohic et al. 2006)], IC 4296 [an FRI radio galaxy with optical line emission and a dusty core], and IC 1459 [which contains detectable HI(Doyle et al. 2005)]. Finally, very little is known about the the outlier S0 galaxy NGC 526 at $\log L_{24} \approx 43.45$,$\log L_{70} \approx 43.0$ in Figure 8.

(bottom panel of Figure 1) – approximately follows the morphological progression along Hubble types. As $\log(L_{24}/L_K)$ and $\log(L_{70}/L_K)$ increase with the specific star-forming rate, the dominant Hubble type becomes progressively later: Sa,Sab → Sb,Scd → Irr. By contrast, most E galaxies lie near the bottom of the banana in a contiguous region of restricted $\log(L_{24}/L_K)$ and decreasing $\log(L_{70}/L_K)$. Some gas-rich E galaxies lie along the star-forming locus of late type galaxies and S0 galaxies are found throughout the banana. Our concern here is to understand the variation of $\log(L_{24}/L_K)$ and $\log(L_{70}/L_K)$ among normal elliptical galaxies in the banana plot.

We show that the banana-shaped correlation, first discussed by TBM09, becomes much tighter when galaxies with AGN emission are removed. Dust grains can be significantly heated by AGN radiation and emit strongly at 24μm within several arcseconds of the galactic centers. These galaxies, having hard, highly concentrated infrared emission, can be identified by the presence of Airy diffraction rings at 24μm. AGN galaxies of all types with Airy rings lie above the infrared banana correlation. To achieve this, centrally illuminated dust would need to move along a trajectory $\delta\log(L_{24}/L_K)/\delta\log(L_{70}/L_K)$ that is steeper than the star formation trajectory along the upper banana, $\delta\log(L_{24}/L_K)/\delta\log(L_{70}/L_K) \approx 1.2$. Because of this slope difference, we suggest that the concentrated source of central IR radiation is due to AGN rather than small starburst regions unresolved at 24μm.

An increasing specific star formation rate from early spiral to irregular galaxies with $L_{24} \propto L_{70}^{1.08}$ apparently explains the progressive transition toward later galactic Hubble types upward along the banana. The bottom part of the infrared banana is populated by elliptical galaxies with a relatively small but significant scatter in 24μm emission, $\log(L_{24}/L_K) \approx 30.15 \pm 0.15$, and a much larger scatter in 70μm emission, $29 \lesssim \log(L_{70}/L_K) \lesssim 31$ in units of (erg s^{-1})$/L_{K\odot}$.

We find that the scatter in $\log(L_{24}/L_K)$ among elliptical galaxies correlates with their stellar metallicity, $(L_{24}/L_K) \propto [Z/H]^{0.7}$. Emission from hotter dust at 24μm is likely to originate in circumstellar regions near AGB stars where dust is thought to be produced. The correlation of 24μm emission with metallicity is probably due to the simple expectation that outflows from metal-rich AGB stars produce more dust per gram of gas ejected.

But the surface brightness variation in 24μm emission from elliptical galaxies, while largely mimicking the de Vaucouleurs profile, contains unexpected color variations when compared with the K-band. When plotted against galactic radius normalized by the K-band effective radius $R/R_e(K)$, the mean $\langle K-24\rangle$ color for a sample of well-observed elliptical galaxies first decreases in a power-law fashion, then undergoes a broad minimum followed by a rise at large radius $R/R_e(K)$. The initial decrease is consistent with decreasing stellar metallicity with radius similar to that found at optical wavelengths, $\Delta[Z/H]/\Delta\log R \approx -0.3$. The origin of the flattening and possible rise in $\langle K-24\rangle$ beyond $R/R_e(K) \sim 1$ is uncertain. If hot dust in AGB winds is thermally heated, increasing $\langle K-24\rangle$ with decreasing stellar metallicity may be related to increasing effective temperature of AGB stars with decreasing metallicity. Alternatively, lower velocity (radiation pressure-driven) outflows from metal poor AGB stars might have larger 24μm emissivity.

The intrinsic scatter of elliptical galaxies in the banana-shaped infrared correlation at longer wavelengths, 70μm and 160μm, is much larger. Recent gas-rich mergers may be a source of cold dust for some elliptical galaxies. However, for most ellipticals we propose that this scatter is due to transient hydrodynamic flows of cold dust from galactic cores far out into the surrounding hot galactic interstellar gas following AGN feedback events. The variation of $\log(L_{70}/L_K)$ is uncorrelated with X-ray luminosity L_X of the galactic/group baryonic halo. The L_{70}/L_K ratios of some group-centered E galaxies like NGC 4472 and 1399 are in good agreement with a steady state model in which dust created by AGB stars is locally destroyed by sputtering at each radius in the galactic atmospheres. Other ellipticals such as NGC 4636 and 5044 have much larger L_{70} luminosities from excess cold dust that cannot be produced by local stars. Lacking convincing evidence of recent gas-rich mergers in these otherwise normal elliptical galaxies, we propose that AGN outbursts cause excess dust to be hydrodynamically transported out to 5-10 kpc into the hot virialized gaseous atmospheres. Spatially extended 70μm emission has been confirmed in relatively nearby elliptical galaxies (TBM07a,b). Evidently, values of L_{70}/L_K for elliptical galaxies along the bottom of the banana plot are transient and may vary on $\sim 10^7$ yr timescales, depending on the grain sputtering time and the AGN duty cycle. The outward relocation of variable masses of cold dust from the central reservoir, observed at different phases of the outflow, may explain why galaxies of similar L_K have L_{70} luminosities that vary over two orders of magnitude.

However, the continuity of the banana plot from E galaxies to early spirals (where L_{24}/L_K and L_{70}/L_K are due to star formation) requires that the enhanced 70μm emission from extended excess cold dust in E galaxies must not exceed L_{70}/L_K as produced by dust in star-forming galaxies of later types. To explain this unlikely coincidence, we speculate that star formation naturally begins in the cores of elliptical galaxies as the mass of accumulated cold gas and dust approaches some star-forming threshold. This conjecture follows from the expected secular accumulation of dust-cooled gas from AGB stellar mass loss in the central ∼kpc of elliptical galaxies (Mathews & Brighenti 2003).

This work is based on observations made with the Spitzer Space Telescope, which is operated by the Jet Propulsion Laboratory, California Institute of Technology, under NASA contract 1407. Studies of the evolution of hot gas in elliptical galaxies at UC Santa Cruz are supported by an NSF grant for which we are very grateful. Support for this work was provided by NASA ADP Grant. F.B. aknowledges financial support from PRIN MIUR 2010-2011, prot. 2010LY5N2T. We acknowledge the usage of the HyperLeda database (http://leda.univ-lyon1.fr) and the NASA/IPAC Extragalactic Database (NED).

REFERENCES

Athey, A., Bregman, J., Bregman, J., Temi, P., Sauvage, M., 2002, ApJ, 571, 272

Birkinshaw, M. Davies, R. L. 1985, ApJ 291, 32

Calzetti, D. et al. 2010, ApJ, 714, 1256

Calzetti, D., et al. 2007, ApJ, 666, 870

Carollo, C. M., Danziger, I. J., Buson, L. 1993, MNRAS, 265, 553

Cristallo, S., Straniero, O., Gallino, R., Piersanti, L., Dominguez, I., Lederer, M.T., 2009, ApJ 696, 797

Crockett, R.M., Kaviraj, S., Silk, J.I., Whitmore, B.C., O'Connell, R.W., et al., 2011, ApJ 727, 115

Davies, R. L., Sadler, E. M., & Peletier, R. F. 1993, MNRAS, 262, 650

Doyle, M. T. et al. 2005, MNRAS 361, 34

Ford, H. A. & Bregman, J. N. 2012, (arXiv1205.1066)

Goudfrooij, P., Hansen, L., Jorgensen, H. E., Norgaard-Nielsen, H. U. 1994, A&A Suppl. Ser. 105, 341

Habing, H. J. 1996, A&A Rev., 7, 97

Kobayashi, C. & Arimoto, N. 1999, ApJ 527, 573

Kobayashi, C. 2004, PASA, 21, 183

Koleva, M., Prugniel, P., De Rijcke, S., Zeilinger, W. W. 2011, MNRAS 417, 1643

Kennicutt, R. C., et al. 2003, PASP, 115, 928

Koprolin, W. & Zeilinger, W. W. 2000, Astron. Astroph. Suppl. Ser. 145, 71

Lauer, T. R., et al. 2005, AJ, 129, 2138

Mathews W.G. 1990, ApJ 354, 468

Mathews, W. G. & Brighenti, F. 2003, ApJ 590, L5

Mehlert, D., Thomas, D., Saglia, R. P., Bender, R., Wegner, G. 2003, A&A, 407, 423

Paturel G., Petit C., Prugniel P., Theureau G., Rousseau J., Brouty M., Dubois P., Cambrésy L., 2003, A&A, 412, 45

Tang, Y., Gu, Q.-S., Huang, J.-S., Wang, Y.-P. 2009, MNRAS 397, 1966

Temi, P., Brighenti, F. & Mathews, W. G. 2009b, ApJ, 707, 890 (TBM09b)

Temi, P., Brighenti, F. & Mathews, W. G. 2009a, ApJ, 695, 1 (TBM09a)

Temi, P., Brighenti, F. & Mathews, W. G. 2008, ApJ, 672, 244 (TBM08)

Temi, P., Brighenti, F. & Mathews, W. G. 2007b, ApJ, 666, 222 (TBM07b)

Temi, P., Brighenti, F. & Mathews, W. G. 2007a, ApJ, 660, 1215 (TBM07a)

Temi, P., Brighenti, F. & Mathews, W. G. 2005, ApJ, 622, 235 (TBM05)

Terlevich, A. I., & Forbes, D. A. 2002, MNRAS 330, 547

Trager, S. C., Faber, S. M., Worthey, G., Gonzalez, J. J., 2000a, AJ 120, 165

Trager, S. C., Faber, S. M., Worthey, G., Gonzalez, J. J., 2000b, AJ 119, 1645

Young, L. M., Bendo, G. J., Lucero, D. M. 2009, AJ 13 7, 3053

Young, L. M. 2002, AJ, 124, 788

van Dokkum, P. G. & Franx, M. 1995, AJ, 11, 2027

TABLE 1
GALAXIES IN FIGURE 1 WITH AIRY DIFFRACTION[a]

Name	T-Type[b]	D (Mpc)	Log L_{Ks} ($L_{Ks,\odot}$)	Log$L_{24\mu m}$ ($erg\ s^{-1}$)	Log$L_{70\mu m}$ ($erg\ s^{-1}$)
NGC 0315	-4	58.9	11.71	42.68	42.77
NGC 0814	-1.8	20.7	9.508	42.65	42.82
NGC 0526	-2.0	78.7	···	43.44	43.02
NGC 1266	-2.1	30.1	10.51	43.07	43.77
NGC 1386	-0.8	16.5	10.56	42.69	42.98
NGC 1377	-2.1	22.2	10.15	43.13	43.2
NGC 2110	-3.0	31.3	11.08	42.97	43.4
NGC 2325	-4.7	31.9	11.2	41.62	41.3
NGC 3226	-4.8	23.5	10.66	41.35	41.97
NGC 3265	-4.8	21.3	9.83	42.3	42.8
NGC 4261	-4.8	31.6	11.44	41.88	41.81
NGC 5077	-4.8	32.4	11.08	41.72	41.85
NGC 6776	-4.1	70.4	11.43	42.08	42.5
NGC 5273	-1.9	16.5	10.32	41.53	41.96
IC 5063	-0.9	45.3	11.16	43.82	43.67
E103-035	-0.3	54.2	10.68	43.87	43.43
ESO428-014	-1.7	21.3	10.5	42.99	43.04

[a] These galaxies are identified with green squares in the central panel of Figure 1.

[b] Morphological type from HyperLeda.

TABLE 2
Relevant Properties of the Trager et al. Sample

Name (NGC)	T-Type[a]	Log L_{Ks} ($L_{Ks,\odot}$)	Log$L_{24\mu m}$ ($ergs^{-1}$)	Log$L_{70\mu m}$ ($erg\ s^{-1}$)	[Z/H][b] ($R_e/8$)	[Z/H][b] ($R_e/2$)	Age[b] (Gyr)	D (Mpc)	$R_e(K)$ ($''$)	$R_e(K)$ (kpc)	R_{max}/R_e[c]
221	-4.7	9.13	39.22	37.93	0.00±0.05	-0.08± 0.05	4.9±1.3	0.81	27.0	0.11	2.72
315[d]	-4.0	11.71	42.68	42.77	0.32±0.06	0.17±0.06	6.9±1.9	58.88	22.2	6.36	0.96
507	-3.3	11.68	42.02	···	0.18±0.06	0.28±0.13	3.5±2.7	67.19	24.0	7.84	1.36
584	-4.6	11.18	41.48	41.18	0.48±0.03	0.26±0.07	3.4±1.1	23.76	23.3	2.69	1.62
636	-4.8	10.67	40.73	···	0.34±0.07	0.10±0.05	6.8±1.4	22.28	15.3	1.66	1.39
720	-4.8	11.14	41.42	40.69	0.44±0.15	1.13±0.42	1.1±0.8	22.29	25.2	2.73	1.57
821	-4.8	10.95	41.06	···	0.22±0.03	0.12±0.05	7.1±1.2	24.09	21.9	2.56	1.07
1374	-4.3	10.68	40.73	···	0.13±0.07	···	9.5±2.6	19.77	15.4	1.48	1.25
1399	-4.5	11.40	41.49	40.50	0.29±0.06	···	11.5±2.4	19.40	32.9	3.10	2.83
1404	-4.7	11.20	41.45	40.80	0.25±0.05	···	9.0±2.5	19.40	18.7	1.76	3.57
1427	-4.0	10.66	40.90	40.89	-0.07±0.03	···	12.2±1.6	23.55	21.5	2.46	1.45
1700	-4.7	11.27	41.51	41.35	0.50±0.03	0.32±0.05	2.8±0.5	38.04	14.9	2.76	1.57
2300	-3.4	11.18	41.36	···	0.36±0.04	0.14±0.04	10.1±2.0	27.67	22.3	2.99	1.54
2778	-4.7	10.26	40.37	···	0.29±0.07	-0.04±0.06	14.9±3.5	22.91	10.5	1.17	1.67
3377	-4.8	10.47	40.50	40.74	0.19±0.06	-0.12±0.04	5.9±1.2	11.22	25.4	1.39	0.76
3379	-4.8	10.89	41.03	40.56	0.21±0.04	0.00±0.04	13.2±2.4	10.57	28.5	1.46	1.09
3608	-4.8	10.83	41.00	41.27	0.26±0.04	0.07±0.07	9.0±2.5	22.91	16.2	1.80	1.44
4261[d]	-4.8	11.44	41.88	41.81	0.18±0.04	-0.01±0.03	21.0±1.7	31.62	24.2	3.72	1.17
4374	-4.2	11.39	41.45	42.03	0.12±0.03	-0.01±0.05	14.4±2.8	18.37	33.5	2.99	1.12
4472	-4.8	11.65	41.71	40.96	0.25±0.05	0.18±0.06	8.4±2.7	17.06	56.1	4.65	0.89
4478	-4.8	10.52	40.74	···	0.29±0.10	-0.01±0.04	10.3±1.7	18.11	11.8	1.04	1.35
4489	-4.8	10.10	40.11	···	0.14±0.06	-0.15±0.04	4.6±0.5	17.86	14.1	1.22	1.13
4552	-4.6	11.03	41.26	41.06	0.27±0.04	0.10±0.04	13.1±2.7	15.34	22.8	1.70	1.65
4649	-4.6	11.52	41.58	40.86	0.27±0.04	0.05±0.04	18.3±2.8	17.06	42.1	3.49	0.46
4697	-4.8	11.22	41.26	41.92	0.06±0.05	-0.29±0.04	15.6±2.5	16.22	39.5	3.11	0.65
5813	-4.8	11.40	41.37	41.51	-0.04±0.03	-0.20±0.06	24.3±2.0	32.21	36.2	5.66	0.95
5831	-4.8	10.84	41.10	···	0.54±0.04	0.18±0.06	4.2±1.0	27.16	19.4	2.56	0.75
5846	-4.7	11.36	41.43	41.53	0.14±0.05	-0.13±0.04	23.1±2.7	24.89	32.7	3.96	2.47
6703	-2.8	11.06	41.34	41.36	0.30±0.06	0.03±0.06	7.9±2.1	32.06	20.1	3.13	1.16
7619	-4.7	11.58	41.62	···	0.20±0.03	0.07±0.04	15.1±2.2	52.97	16.4	4.22	1.64
7626	-4.8	11.34	41.44	41.17	0.16±0.04	-0.06±0.02	18.2±2.0	39.99	20.7	4.02	1.13
7785	-4.8	11.46	41.58	41.45	0.20±0.04	-0.01±0.04	15.0±2.3	55.46	17.2	4.64	0.84

[a] Morphological type from HyperLeda.

[b] Values of $[Z/H]$ for $R_e/8$ and $R_e/2$ are "model 4" values from Trager et al. (2000a,b) refer to the B-band effective radius R_e which on average is about 1.45 times larger than the K-band value $R_e(K)$ (TBM08). Ages listed above refer to the $R_e/2$ observations.

[c] Maximum extent of observable 24μm emission.

[d] Identified as an AGN galaxy from 24μm Airy rings.

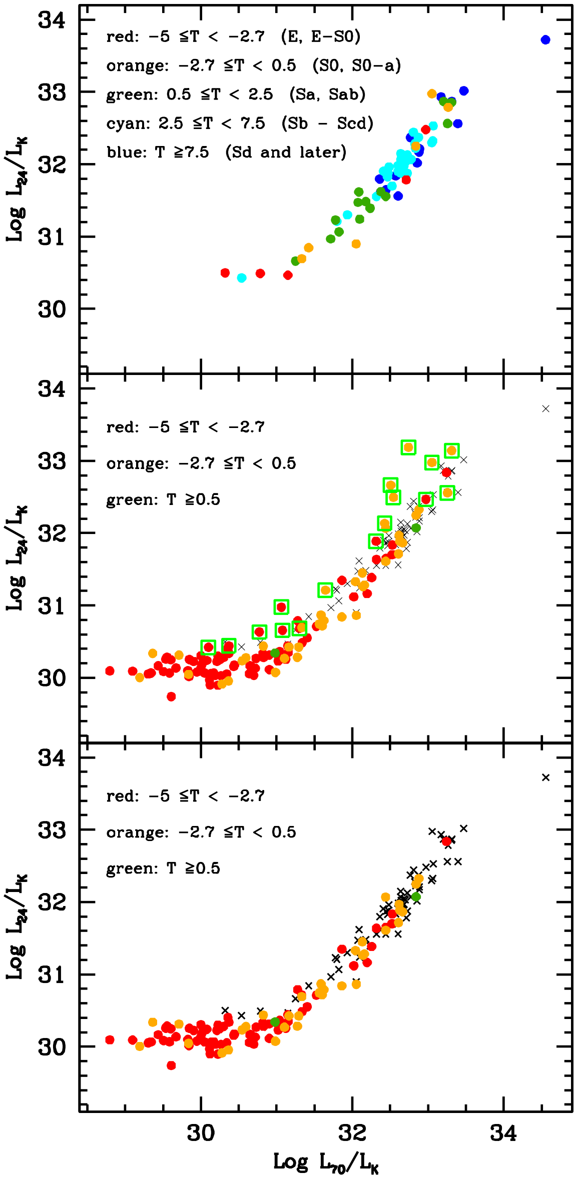

FIG. 1.— Upper panel: Infrared color-color banana plot L_{24}/L_K vs. L_{70}/L_K for SINGS galaxies showing progression of Hubble types. Central panel: IR color-color plot showing galaxies in the TBM09b sample with X indicating SINGS galaxies. Green squares indicate TBM09b (AGN or starburst) galaxies with centrally concentrated 24μm emission. Bottom panel: Same as central panel without galaxies having centrally concentrated 24μm emission.

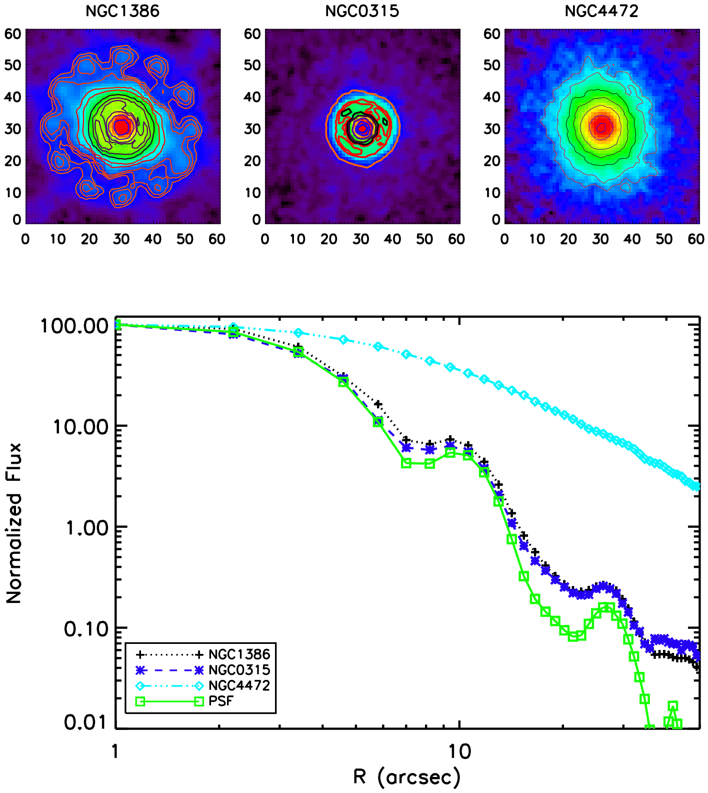

Fig. 2.— Upper panels: 24μm images of NGC 1398 and 315 showing Airy diffraction rings and NGC 4472 with diffraction-free image. The colors and contours are qualitative only, intended to illustrate non-axisymmetric features in the diffraction pattern. Lower panel: Azimuthally averaged radial diffraction fluxes at 24μm for the three galaxies imaged above: NGC 1386 (black dotted line); NGC 0315 (blue dashed line); NGC 4472 (light blue long dash-triple dotted line). For comparison we plot the point response function of the Spitzer telescope at 24μm (green solid line). All fluxes are normalized to 100 (in arbitrary units) at one arcsecond.

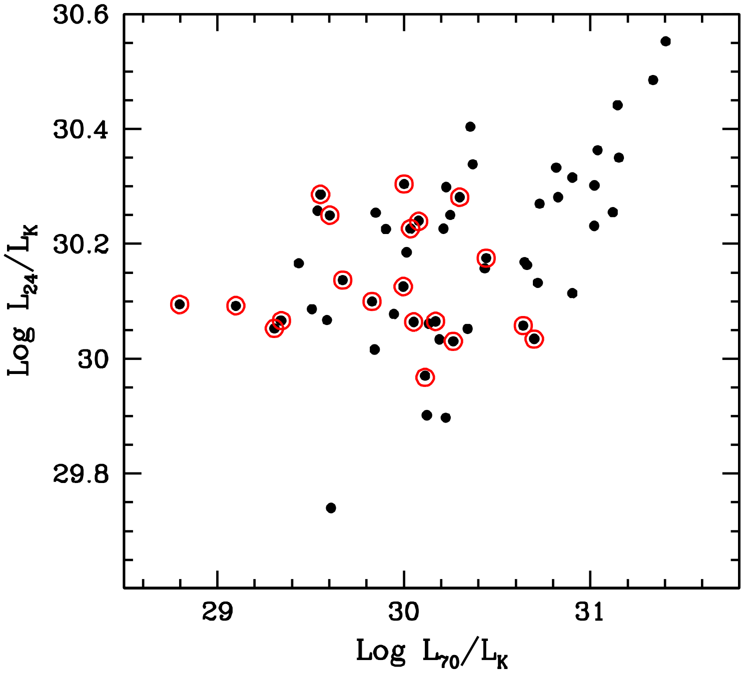

FIG. 3.— Expanded view of E and E-S0 galaxies (with $T < -2.7$) at the bottom of the banana plot, omitting AGN galaxies with significant point source emission at 24μm. Red circles identify a subset of these galaxies that are also in the sample of Trager et al. (2000a, b) which have been observed at both 24 and 70μm but omitting two that are identified as AGNs in Table 1, NGC 0315 and NGC 4261.

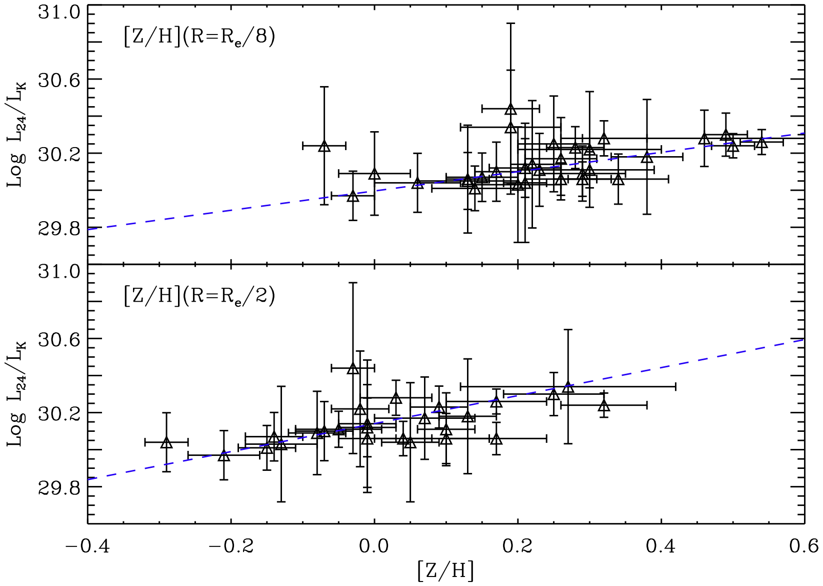

Fig. 4.— Correlation between L_{24}/L_K and stellar metallicity $[Z/H]$ for the Trager et al. (2000a, b) sample of E galaxies. Upper and lower panels show the linear relation with metallicities values derived in the $R_e/8$ and $R_e/2$ aperture respectively where R_e is the effective radius in the B-band. Two galaxies identified as AGNs in Table 1 (NGC 315 and NGC 4261) are not included in either panel. In the lower panel we also exclude the outlying (and very uncertain) value $[Z/H] = 1.13$ for NGC 720.

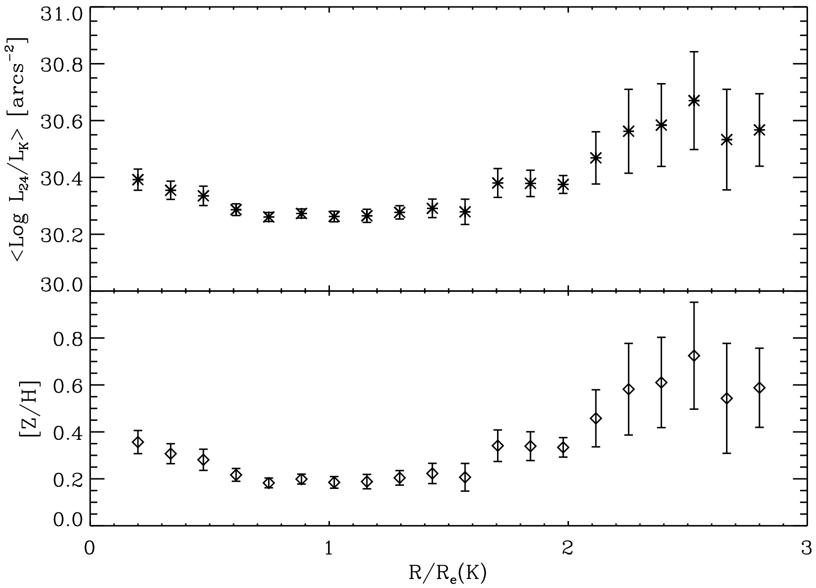

FIG. 5.— Upper panel: Variation of Trager sample-averaged radial color profile (in surface brightness units) with galaxy radius normalized to the K-band half light radius $R_e(K)$. Lower panel: Variation of Trager sample-averaged radial stellar metallicity profiles found using the correlation in Figure 4 derived for the $R_e/2$ aperture.

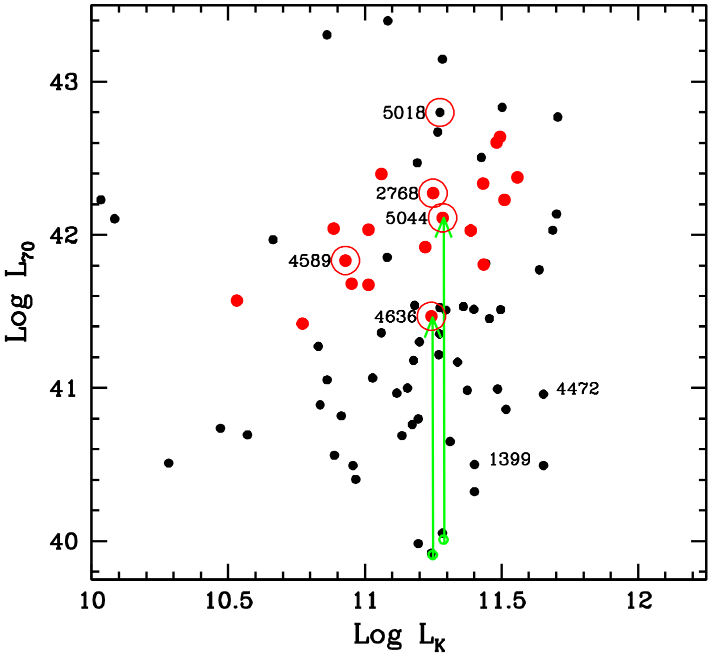

FIG. 6.— Plot of L_{70} vs. L_K for elliptical galaxies ($T < -3.5$) in the TMB09b sample. Galaxies marked in red all have excess extended dust and the large red circles indicate galaxies in which the spatial extension has been observed at 70μm. Vertical green arrows show the approximate estimated increase in L_{70} due to excess cold dust in NGC 5044 and 4636.

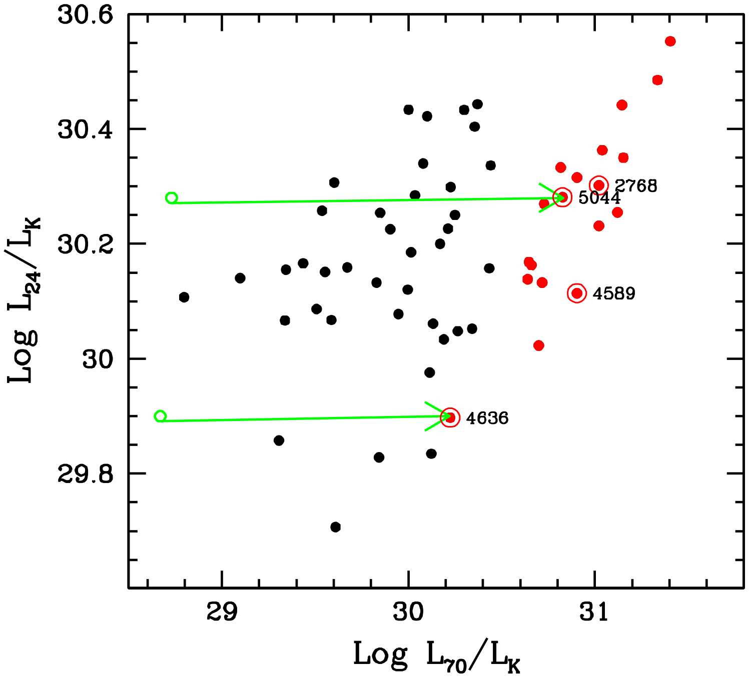

Fig. 7.— Infrared color-color plot as in Figure 3 showing only E and E-S0 galaxies with $T \leq -3.5$. Galaxies in red and circled in red are identical with those in Figure 6, but now appear along the right boundary of the lower banana. As in Figure 6 the horizontal green arrows show the trajectories of NGC 5044 and 4636 when extended cold dust is added to 70μm emission produced only by local AGB stellar mass loss.

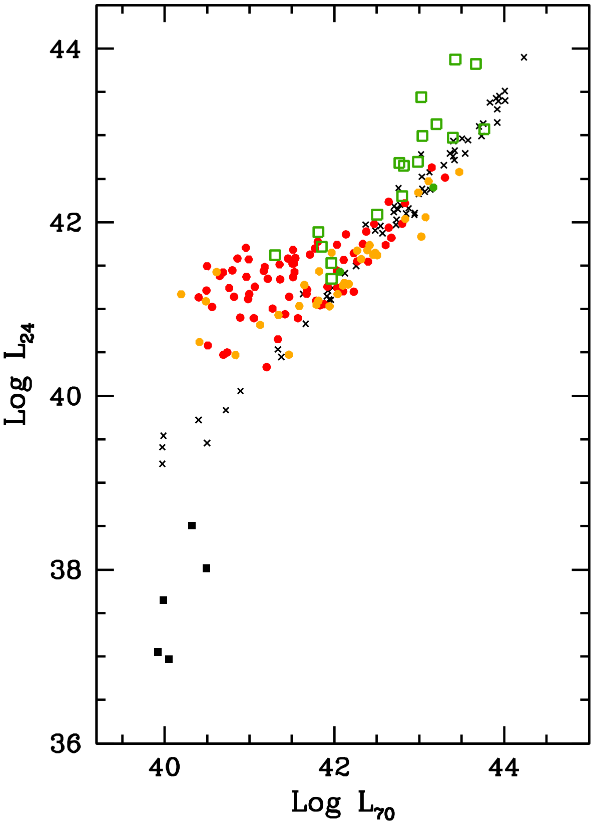

FIG. 8.— Plot of L_{24} against L_{70} as in the bottom panel of Figure 1 but without the L_K normalization. Symbols are identical to those in that panel. Filled squares show computed steady-state emission from diffusely distributed interstellar dust in five representative elliptical galaxies (NGC 4472, 1404 4636, 1399 & 5044 in order of decreasing L_{24}). The star formation locus of SINGS galaxies (crosses) is $L_{24} \propto L_{70}^{1.08}$.